JOURNAL OF GUIDANCE, CONTROL, AND DYNAMICS
Vol. 19, No. 3, May–June 1996

Nonlinear Flutter Analysis of Missiles with Pneumatic Fin Actuators

E. Yehezkely* and M. Karpel†
Technion—Israel Institute of Technology, Haifa 32000, Israel

A method for flutter analysis and design of missiles with pneumatic fin actuators is presented. The method combines state–space aeroelastic models with nonlinear pneumatic models for time-domain simulations and for frequency-domain approximate solutions. The missile and its fins are represented by normal modes with the generalized unsteady aerodynamic force coefficients approximated by rational functions. Time simulations are presented for various velocities, maneuver commands, and pneumatic parameters, and the system behavior at the flutter boundary is discussed. It is shown that the fundamental fin flutter speed is strongly dependent on the missile maneuver commands. The flutter mechanism is investigated with equivalent frequency-domain modes. A way to increase the flutter speeds by introducing chordwise-bending flexibility near the fin trailing edge is introduced and demonstrated.

Introduction

THE flexible missile structure, when subjected to high-velocity flow, may experience flutter, a dynamic aeroelastic phenomenon in which the structural vibrations become unstable at a certain velocity. Flutter in air-to-air missiles is affected mainly by the structural and aerodynamic properties of the fins, and the mechanical properties of the actuators, whereas the missile body usually has a minor role. Body modes may become important in flutter analysis of long flexible missiles. It is important to design the fins and their actuators such that flutter will not occur in the flight envelope.

The fin actuator maneuvers the missile according to command signals from the control system. There are three types of actuator systems: hydraulic, electromechanical, and pneumatic. Hydraulic and electromechanical actuators are basically position-control actuators, where the fin angle is monitored by closed-loop control. The mechanical nonlinearities in these systems are mainly a result of free play in a small portion of the actuator stroke, when the hinge moment becomes zero. At other parts of the motion, the actuator mechanical properties can be assumed to be linear, with negligible influence of the external loads on the actuator dynamics (irreversibility). These characteristics enable the analysis of the system to be performed by frequency-domain methods.[1–4]

The desire for inexpensive, fast-reaction actuators, with small volume and weight, expanded the use of pneumatic systems.[5] Typical pneumatic actuators are basically hinge-moment control actuators. The fin hinge moment needed for maneuverability is obtained by a pair of pistons; one supplies hinge moment opposite to the other. Each piston has an electrical solenoid with two positions, one filling and one emptying the cylinder. A typical filling-emptying actuator pneumatic frequency is 25 Hz. The pressure in the cylinder that provides the hinge moment is controlled by the duty cycle (DC), which is the ratio between the filling time and the total cycle time. The nonlinearity and reversibility of pneumatic actuators are significantly more dominant than those of hydraulic and electrical ones. The combination of the flexible structures and the unsteady aerodynamics with nonlinear reversible pneumatic systems raises the need for time-domain analysis.

Dynamic response analysis is commonly based on the modal approach[6] in which the structural displacements are represented by a set of low-frequency natural vibration modes, which serve as generalized coordinates. While a typical discrete-coordinate finite element model may have thousands of degrees of freedom, a typical generalized-coordinate equation of motion for aeroelastic stability and response analysis is usually based on a small number of modes with a negligible reduction in accuracy. Unsteady aerodynamic force coefficient matrices, normally available as transcendental functions of the harmonic vibration frequency, can be evaluated by a variety of computer codes.[7] To allow time-domain, state–space formulation, these matrices have to be approximated by rational functions of the Laplace variable s (Refs. 8 and 9).

Structural Equations of Motion

The discrete matrix equation of motion of an n-degree-of-freedom nominal structure is

$$[M]\{\ddot{u}(t)\} + [B]\{\dot{u}(t)\} + [K]\{u(t)\} = \{F_a(t)\} + \{F_p(t)\} \quad (1)$$

where $\{u\}$ is the discrete-coordinate displacement vector; $[M]$, $[B]$, and $[K]$ are the finite element mass, damping, and stiffness matrices; $\{F_a\}$ is the vector of distributed aerodynamic forces; and $\{F_p\}$ is the vector of local pneumatic forces. As detailed below, both $\{F_a\}$ and $\{F_p\}$ are functions of the structural response. The fins are connected to the structural model of the missile body in all directions except in pitch rotation. The pneumatic force vector $\{F_p\}$ is entirely zero except for two equal pitching moments for each actuator, with opposite signs, applied on the fin hinge and on the actuator backup structure. The common modal approach transforms Eq. (1) to modal coordinates by assuming that the structural displacement vector $\{u\}$ is a linear combination of a limited set of low-frequency vibration modes:

$$\{u(t)\} = [\Phi]\{\xi(t)\} \quad (2)$$

where $\{\xi(t)\}$ is the vector of generalized displacements and $[\Phi]$ is the matrix of low-frequency modal deflections which serve as generalized coordinates. The modes include missile rigid-body modes (when applicable) and fin rigid-body pitch-rotation modes. Substitution of Eq. (2) in Eq. (1) and premultiplication by $[\Phi]^T$ yield the modal equation of motion

$$[M_n]\{\ddot{\xi}(t)\} + [B_n]\{\dot{\xi}(t)\} + [K_n]\{\xi(t)\} = \{F_{na}\} + \{F_{np}\} \quad (3)$$

where $[M_n]$, $[B_n]$, and $[K_n]$ are the generalized mass, damping, and stiffness matrices and $\{F_{na}\}$ and $\{F_{np}\}$ are the generalized vectors of aerodynamic and pneumatic forces. Since the driven fins are not connected in pitch to the body when the modes are generated, their torsional properties might not be adequately represented in the low-frequency modes included in $[\Phi]$. This difficulty can be overcome by calculating the modes with each driven fin root loaded with a relatively large fictitious pitch inertia term. The added inertia causes the modes that serve as generalized coordinates to include more fin torsion. The effects of the fictitious moments of inertia can be

Received Jan. 3, 1995; revision received May 15, 1995; accepted for publication Dec. 3, 1995.

*Graduate Student, Aerospace Engineering Department.
†Associate Professor, Faculty of Aerospace Engineering. Member AIAA.

removed when Eq. (3) is constructed using the fictitious-mass technique of Ref. 10. This technique was demonstrated in Ref. 11 in cases of large stiffness variations.

Common linear unsteady aerodynamic codes can be used to calculate the complex generalized force coefficient matrices $[Q(ik)]$ for harmonic oscillations at various reduced frequencies $k = \omega b/U$, where b is a reference semichord and U is the true airspeed. The generalized aerodynamic forces are related to the frequency-domain generalized displacements by

$$\{F_{na}(ik)\} = q[Q(ik)]\{\xi(ik)\} \tag{4}$$

where q is the dynamic pressure.

Aerodynamic approximation schemes[8,9] can be used to approximate $[Q(ik)]$ by rational functions in the frequency domain and then to expand it to the Laplace domain by replacing ik with s, which yields the general form

$$[Q(ik)] \cong [A_0] + (b/U)[A_1]s + (b^2/U^2)[A_2]s^2 + [D]([I]s - (U/b)[R])^{-1}[E]s \tag{5}$$

where the coefficient matrices are optimized to fit the oscillatory data in the least squares sense. References 8 and 9 use Eq. (5) to construct the linear state–space aeroelastic equation of motion. At high Mach numbers, the unsteady aerodynamics are often based on piston theory,[6,7] which is, in fact, a theory where $[Q(ik)]$ is a linear function at k:

$$[Q(ik)] = \left[Q^{(R)}\right] + ik\left[Q^{(I)}\right] \tag{6}$$

where $[Q^{(R)}]$ and $[Q^{(I)}]$ are the real and imaginary parts of $[Q(ik)]$ calculated at $k = 1$. The replacement of ik in Eq. (6) by s yields the time-domain piston theory generalized aerodynamic forces

$$\{F_{na}\} = q\left[Q^{(R)}\right]\{\xi\} + (qb/U)\left[Q^{(I)}\right]\{\dot{\xi}\} \tag{7}$$

The substitution of Eq. (7) in Eq. (3) gives

$$[M_n]\{\ddot{\xi}(t)\} + [\bar{B}]\{\dot{\xi}(t)\} + [\bar{K}]\{\xi(t)\} = \{F_{np}\} \tag{8}$$

where

$$[\bar{B}] = [B_n] - (qb/U)\left[Q^{(I)}\right], \qquad [\bar{K}] = [K_n] - q\left[Q^{(R)}\right]$$

The new generalized stiffness and damping matrices $[\bar{B}]$ and $[\bar{K}]$ contain not only the structural elements but also the aerodynamics stiffness and damping. Equation (8) can be put in the standard first-order state–space form

$$\{\dot{x}(t)\} = [A]\{x(t)\} + \{b(t)\} \tag{9}$$

where

$$\{x\} = \begin{Bmatrix} \xi \\ \dot{\xi} \end{Bmatrix}, \qquad [A] = \begin{bmatrix} [0] & [I] \\ -[M_n]^{-1}[\bar{K}] & -[M_n]^{-1}[\bar{B}] \end{bmatrix}$$

$$\{b\} = \begin{Bmatrix} 0 \\ [M_n]^{-1}\{F_{np}\} \end{Bmatrix}$$

where the system matrix $[A]$ is constant. The forcing vector $\{b(t)\}$ depends on the nonlinear dynamics of the pneumatic system, which is a function of the control command and the structural displacements and velocities.

A simple numerical solution of Eq. (9), which assumes constant time steps Δt and small variations of $\{b(t)\}$ during a time step, is

$$\{x((n_t+1)\Delta t)\} = e^{[A]\Delta t}\left(\{x(n_t\Delta t)\} + [A]^{-1}\{b(n_t\Delta t)\}\right) - [A]^{-1}\{b(n_t\Delta t)\} \tag{10}$$

where n_t is the sequential step number. This is the exact response at time $(n_t+1)\Delta t$ to the constant excitation $\{b(n_t\Delta t)\}$ with the initial condition $\{x(n_t\Delta t)\}$.

Mathematical Model of the Pneumatic Actuator

A conventional missile is maneuvered by two pairs of movable fins in perpendicular planes. Each pair is driven by an actuator through a torque shaft about which the two fins rotate. The purpose of this section is to describe the mathematical model of a typical, pneumatic system, based on Ref. 1, and the way it can be coupled with the aeroelastic equations of motion. The pneumatic actuator is built of two cylinders that push pistons by gas pressure in turns, one to the positive and one to the negative rotation angle. Each cylinder has a solenoid valve with two positions, one that lets the gas flow from a high-pressure reservoir into the cylinder through an orifice and one that releases gas from the cylinder to the atmosphere. Electrical pulses to the solenoid control the valve position which typically changes 15–40 times per second. The valve motion is so fast that the change can be considered instantaneous in our applications. The percentage portion of gas filling time in one cycle is called the DC:

$$DC = \frac{T_{DC}}{T_{\text{cycle}}} \times 100\% \tag{11}$$

The hinge moment is determined by the pressure in the cylinder, which is increased with increasing DC. This kind of control is called pulse width modulation.

The gas equation of state relates the static pressure P, volume V, mass G, and temperature T of the gas in the cylinder by the gas constant normalized to the molecular weight (R). For ideal gases this is

$$PV = GRT \tag{12}$$

For our purposes the flow is considered isentropic and isothermal. The flow of gas through the converging orifices depends upon some constants (cross-section area, temperature, kind of gas) and the pressure at the inlet P_u and outlet P_d of the orifice. The rate of flow changes with the ratio between P_u and P_d for output pressure larger than

$$P_{CR} = P_u[2/(k_c+1)]^{k_c/(k_c-1)} \tag{13}$$

where k_c is the ratio of specific heats. For smaller outlet pressure, the flow is choked, that is, depends on the inlet pressure only. The nonlinear flow equation may be expressed by

$$\dot{G} = C_d C_2 A_d P_u f/\sqrt{T} \tag{14}$$

where C_d is the orifice constant, A_d is its outlet area, and

$$f = f\left(\frac{P_d}{P_u}\right) = \begin{cases} \dfrac{C_1}{C_2}\left(\dfrac{P_d}{P_u}\right)^{1/k_c}\sqrt{1-\left(\dfrac{P_d}{P_u}\right)^{(k_c-1)/k_c}} & @\ P_d \geq P_{CR} \\ 1 & @\ P_d < P_{CR} \end{cases}$$

$$C_1 = \sqrt{\frac{2k_c}{(k_c-1)R}}; \qquad C_2 = \sqrt{\frac{k_c}{R[(k_c+1)/2]^{(k_c+1)/(k_c-1)}}}$$

The inlet and outlet pressure values of the filling orifice are $P_u = P_s$ and $P_d = P$, where P_s is the supplied pressure, and those of the emptying orifice are $P_u = P$ and $P_d = P_{\text{atm}}$, where P_{atm} is the atmospheric pressure. The actuator dynamics are coupled with the structural dynamics through the piston motion, which is kinematically related to the differential rotation between the fin root and the missile-body actuator attachment point. The cylinder gas mass G is found by numerical integration of Eq. (14), taking into account the valve position based on DC of Eq. (11). The cylinder pressure P is calculated in each step by Eq. (12) with the volume V defined by the piston travel.

The pneumatic hinge moment (M_p), which appears in the nonzero element in $\{F_p\}$ of Eq. (1), depends on the pressure in the cylinder,

the area of the piston ($\bar{A}$), the actuator arm (d), and the O-ring friction:

$$M_P = (P - P_{\text{atm}})\bar{A}d \pm F_{\text{fr}}d \tag{15}$$

where the sign of the friction force (F_{fr}) is defined by the piston movement. The friction force, caused by the contact between the O-ring around the piston and the cylinder, depends on the initial assembly pressure on the O-ring, P_s, and on the dynamic friction, which is assumed here to be linearly dependent on the pressure in the cylinder:

$$F_{\text{fr}} = f_1 P_s \bar{A} + f_2 P \bar{A} \tag{16}$$

where f_1 and f_2 are the static and dynamic friction coefficients.

Models for Numerical Applications

Models of a clamped fin and of a complete missile that were used for numerical applications are shown in Fig. 1. The models were built by means of finite elements, for the computation of the natural modes and the associated generalized aerodynamics, at various supersonic Mach numbers at altitude of 8000 m by the piston theory method, using MSC/NASTRAN.[7] The clamped fin is connected to the ground in all directions except for pitch rotation about the hinge line, which is controlled by a pneumatic actuator. The full missile has eight fins but only the four forward ones are movable. The model for symmetric maneuvers in the x–z plane is of the right side of the missile with one movable and one fixed fin. The movable fin is structurally connected to the missile body in all directions except pitch. The aerodynamic panel model of each fin is based on six spanwise and four chordwise divisions. The body aerodynamics were modeled with dummy aerodynamic panels with areas tuned to match slender-body lift coefficient.

The pneumatic system uses nitrogen as an actuation gas with a supply pressure of 58 atm. The piston area is 1.1×10^{-4} m^2 in the clamped model and 6.0×10^{-4} m^2 in the full-missile case. The simulation models were based on 5 modes for the clamped-fin case, including one rigid-body pitch rotation, and 13 symmetric modes for the complete-missile case, including 3 rigid-body modes (heave, pitch, and rigid-body pitch of the forward fin). The lowest elastic natural frequency in the clamped-fin case, which corresponds to the first fin bending, was 202 Hz. The lowest elastic natural frequency in the full-missile case, which corresponds the first body bending, was 28 Hz. The first bending frequency of the movable fin in this case was 233 Hz (the ninth elastic frequency). Analyses with more modes taken into account did not exhibit significant differences. The inclusion of fictitious fin-root inertia to have the fin torsional properties represented in the low-frequency modes, as discussed after Eq. (3), was found to be not important in our cases because, as shown below, the flutter mechanisms do not include significant fin torsion.

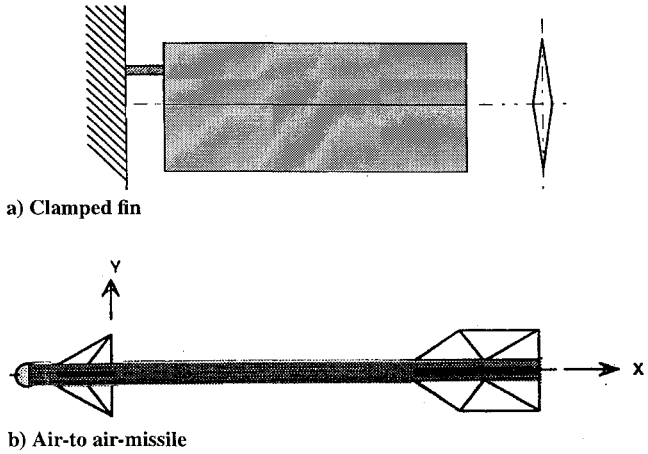

Fig. 1 Test-case models.

Time Response to Pneumatic Step Commands

Time-response analyses for the coupled structural pneumatic system were performed with the two models by numerical solution of Eq. (9) using Eq. (10) with $\Delta t = 10^{-4}$ s. Analyses with smaller time steps gave identical results. The structural initial conditions in all the cases were $\{x(0)\} = \{0\}$, and the initial pressure in the cylinder was $P(0) = P_{\text{atm}}$, namely zero hinge moment. A step command in our context means a jump of DC at $t = 0$ from zero to a constant positive percentage value. Time-response curves of the pitch angle at the root of the clamped fin at $U = 500$ m/s to pneumatic step commands with $DC = 20$ and 40% are shown in Fig. 2. Each saw tooth is the response in a pneumatic cycle of 0.04 s. The cycle starts with flow into the cylinder (for 20 or 40% of the cycle time), which pushes the fin angle up, and ends with flow from the cylinder to the atmosphere, which lets the aerodynamic hinge moment push the fin angle back. Steady state is achieved in each case after about 0.35 s with constant saw-tooth pneumatic oscillations about a mean value. Small sinusoidal structural oscillations of about 100 Hz can also be observed on top of the pneumatic ones.

Figure 3 shows the time history of the pitch angle with the same conditions as in Fig. 2 but at $U = 545$ m/s. At $DC = 20\%$, the structural oscillations are larger than in Fig. 2, but the system is still stable. At $DC = 40\%$, the system is unstable and exhibits a diverging flutter behavior. Although it is obvious that the first case is stable and the second unstable, the pneumatic oscillations do not allow easy determination of the structural damping by the curve-fitting methods used to define the flutter boundary in time-marching solutions. The 40% case is also shown in Fig. 4 for a slightly smaller velocity of $U = 540$ m/s. The beating phenomenon shown in Fig. 4 is caused by the interaction between the fin rigid-body pitch and bending modes, whose frequencies get close to each other when flutter is approached, as discussed below. The appearance of beating response can serve as a warning signal before the destructive flutter occurs. In our work we define the flutter boundary by the conditions at which the beating response occurs. To find the beating onset speed, computations were first performed with DC increments of 5% and velocity increments of 5 m/s. When, for a certain DC value, the response changed from converging to diverging, computations with intermediate velocity increments of 1 m/s were performed until beating appeared.

The variation of flutter speed of the clamped fin with the duty cycle is shown in Fig. 5 for no-friction and friction cases. The friction case is with realistic friction coefficients of $f_1 = 0.06$ and $f_2 = 0.08$ in Eq. (16). The graphs imply that the flutter speed of a maneuvering missile can be significantly lower than that of level flight, when the hinge moments are very small. The minimal flutter velocities are reached here at $DC = 25$–40%. The small variation of the flutter velocity at high DC values occurs because the pressure in the cylinder asymptotically approaches its maximum value. The

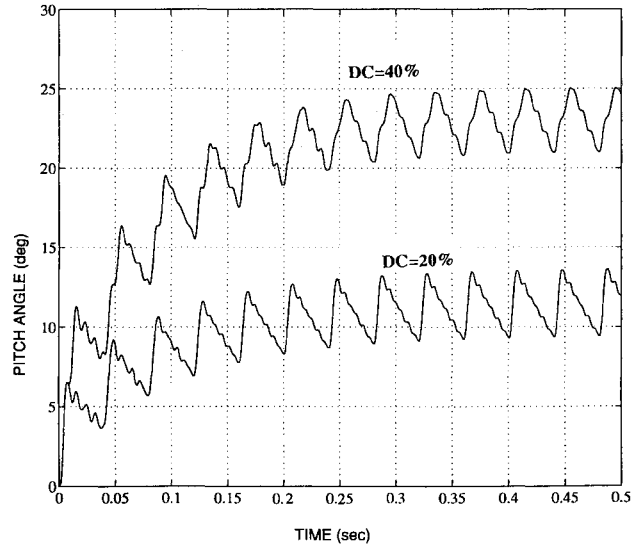

Fig. 2 Fin angle response to step command at $U = 500$ m/s.

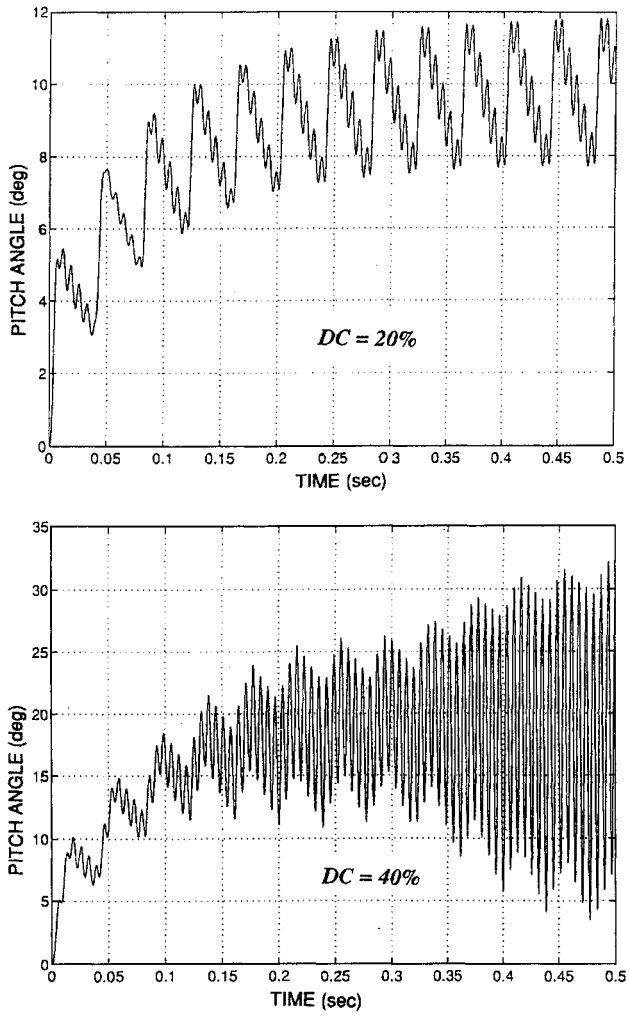

Fig. 3 Fin angle response to step command at $U = 545$ m/s.

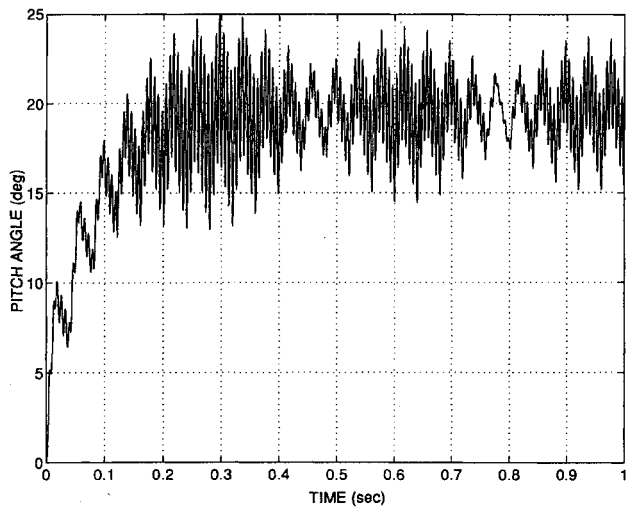

Fig. 4 Fin angle response to step command at $U = 540$ m/s, $DC = 40\%$

amplitudes of the pneumatic oscillations about the mean values in the no-friction case (not shown) become significantly smaller than those with no friction in Fig. 2. The friction flutter velocities are larger than those without friction by 20% and more, but the sensitivity of flutter velocity to the actuator hinge moment is also larger.

Equivalent Linear System

It is desirable to replace the pneumatic system by equivalent spring and damper such that the entire system becomes linear.

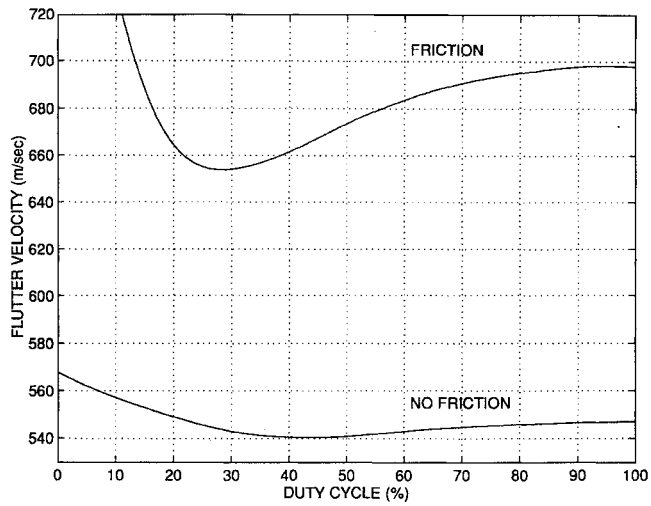

Fig. 5 Flutter velocity vs DC, no-friction, and friction cases.

Frequency-domain or root-locus methods can then be applied more efficiently and with better understanding of the flutter mechanism. Equivalent rotational springs (K_θ) were determined in our work from the ratio P/V between the pressure and the volume of the gas in the cylinder at the steady-state parts of selected stable time simulations:

$$K_\theta = \frac{d^2 \bar{A}^2 P}{V} \tag{17}$$

Since the value of P/V oscillates at steady state, equivalent-system analyses can be performed with K_θ determined by the maximal, mean, and minimal values of P/V at steady state. Vibration modes of a linearized system are determined with the fin root attached to the missile body (or the ground in the clamped-fin case) such that an elastic fin pitch mode replaces the fin rigid-body mode. Flutter analysis can then be performed by root-locus analysis of the system matrix $[A]$ of Eq. (9), with varying dynamic pressure, or by the classical U-g or p-k methods.[7]

Flutter occurs in linearized root-locus analysis when a root branch crosses to the right side of the Laplace domain. Figure 6 shows the resulting flutter velocities vs DC of the equivalent clamped fin with no damping, in comparison with the no-friction time-domain results of Fig. 5. When DC increases in the equivalent cases, the larger equivalent stiffness values because of higher pressure in the cylinder cause lower flutter speeds. The equivalent stiffness, which is based on the maximum P/V response, is more conservative and gives more accurate results up to $DC = 55\%$, which is the range in which pneumatic actuators normally operate. The pneumatic damping resulting from flow through the emptying orifice in the nonlinear analysis is negligible at low DC values but becomes more significant at higher values, when the pressure is high and the outlet flow is choked. Figure 6 shows that the use of equivalent springs might be inaccurate and hence might require higher safety margins.

Figure 7 shows the root loci of the first two modes, pitch and bending, with varying dynamic pressure, calculated with an equivalent spring based on a maximal P/V response value with $DC = 20\%$. The fin pitch frequency increases with the increased dynamic pressure and gets close to the bending frequency, and the two modes interact to produce flutter. It is clear that as the equivalent spring stiffness increases, because of increased DC value, the pitch mode starts at a higher frequency; thus the branches of pitch and bending get closer and produce flutter at a lower dynamic pressure.

Time-response simulations were also performed with the linear model, starting from some nonzero modal deformations. The response in these cases exhibited smooth converging or diverging oscillations, except for beating oscillations just below the stability boundary, which indicates that the beating shown above was not a result of system nonlinearity.

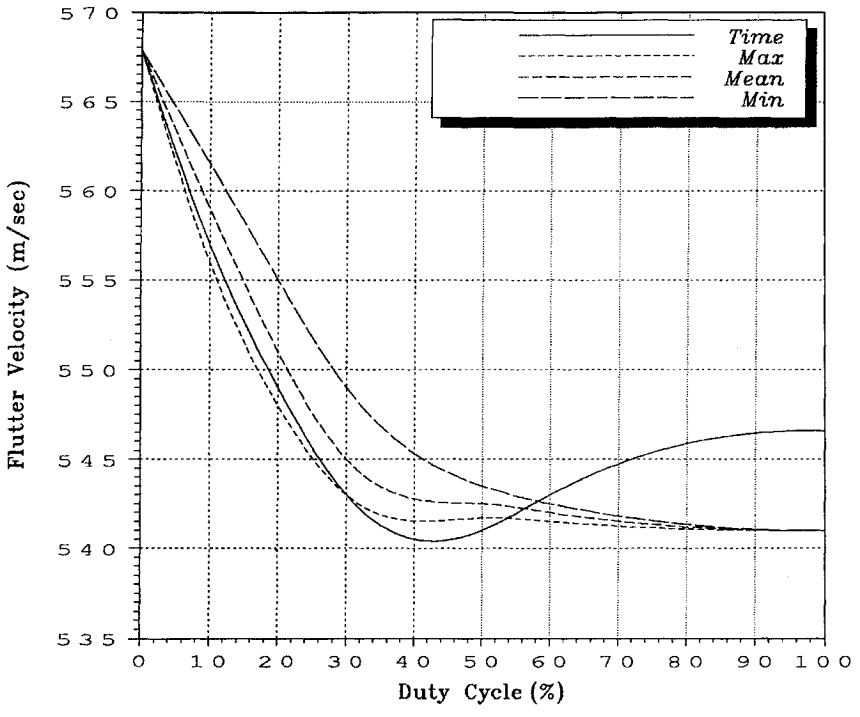

Fig. 6 Flutter velocity vs *DC*, linearized, and nonlinear solutions.

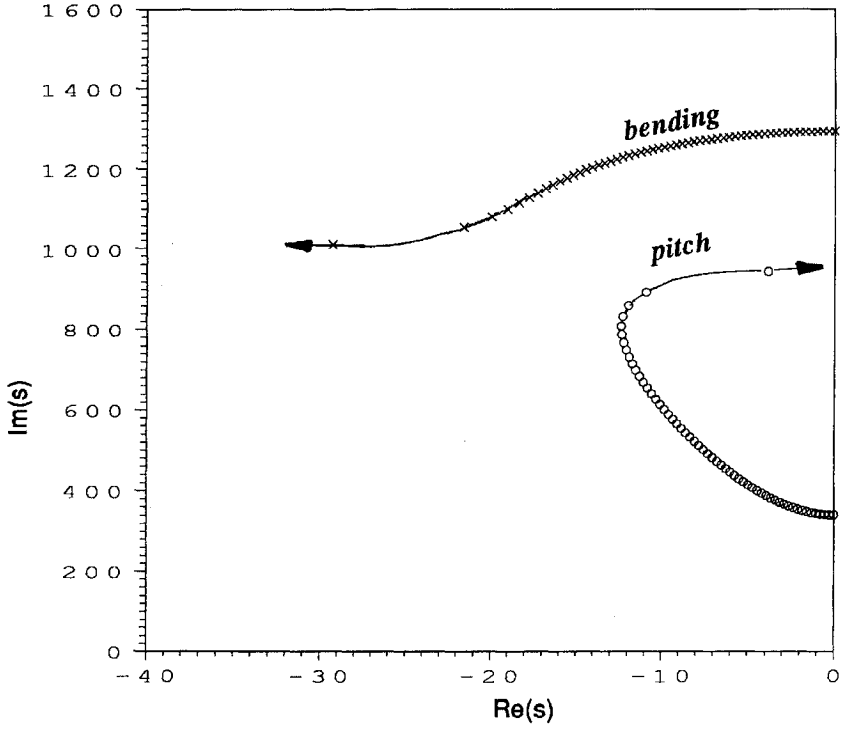

Fig. 7 Root loci of the clamped fin with equivalent spring.

Structural Means to Increase Flutter Velocity

The low fin-pitch frequency cannot be avoided when pneumatic actuation is used. We can increase the flutter velocity by designing the pneumatic system to have high damping, but that might degrade the system performance. Another approach is to reduce the rate of frequency increase with increasing dynamic pressure, such that it will start to interact with the bending frequency at higher speeds. This can be accomplished by reducing the aerodynamic hinge moment resulting from pitch rotation. This moment is high at supersonic flight because the aerodynamic center of the fin moves backwards, whereas the hinge line must be located forward of the subsonic aerodynamic center to avoid subsonic divergence.

The high supersonic hinge moments may also impose other costly design constraints on the actuator, such as a requirement for high supply pressure. Dillenius et al.[12] proposed a way to reduce the hinge moments by introducing chordwise flexibility near the fin trailing edge. They showed that this flexibility causes static aeroelastic effects, which move the supersonic aerodynamic center forward significantly, while the motion of the subsonic center is very small. We used this idea in our work as a means to increase the flutter velocity by reducing the aerodynamic stiffness.

Reference 12 increased the chordwise flexibility by introducing spanwise slits at the rear part of the fin. We simulated these effects by reducing Young's modules of the rear half of the clamped-fin

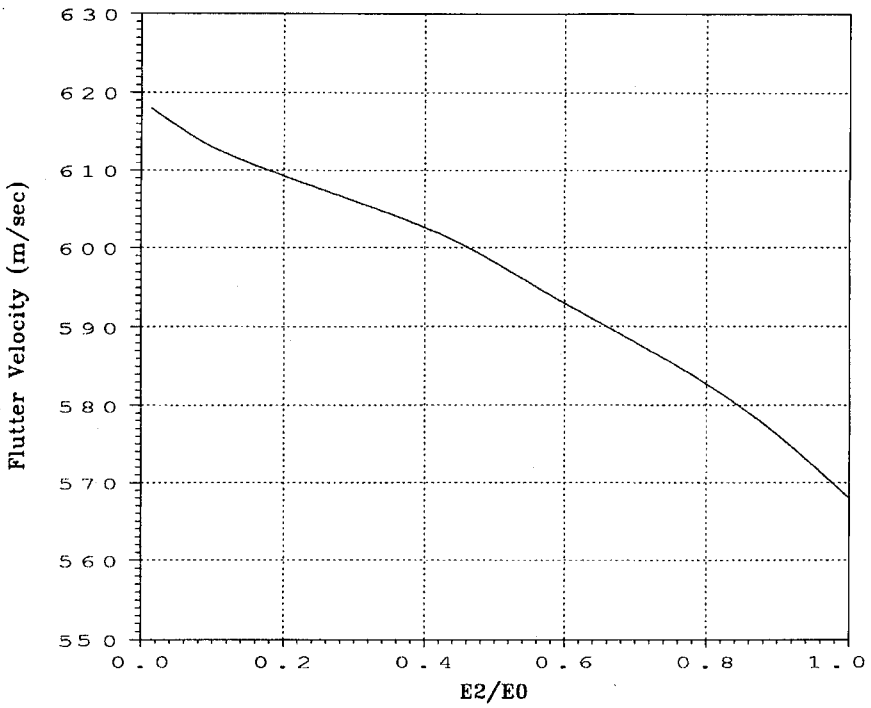

Fig. 8 Flutter velocity vs rear-part stiffness ratio, $DC = 0$.

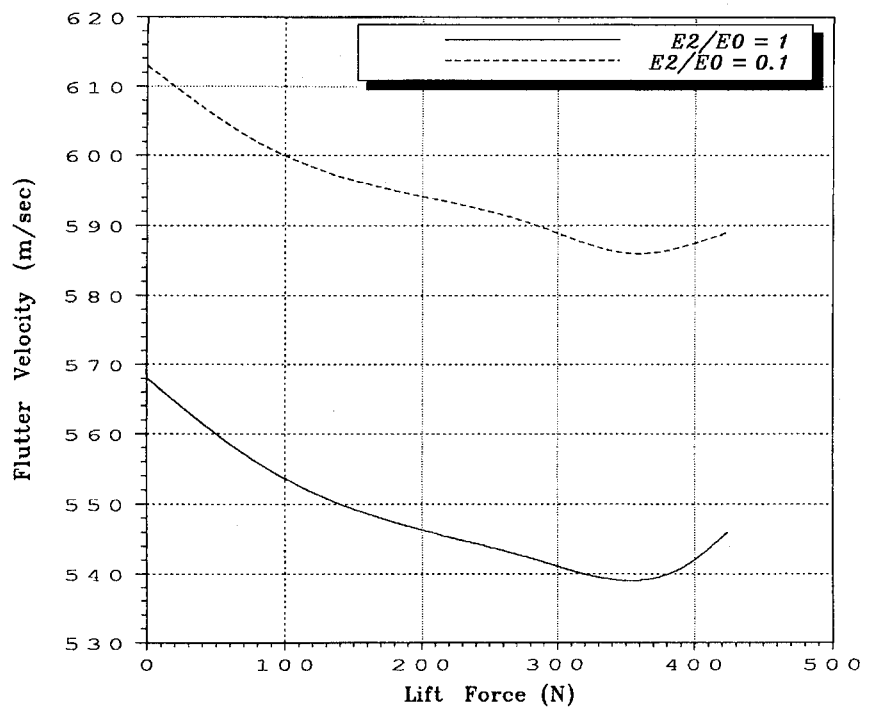

Fig. 9 Flutter velocity vs commanded fin lift, nominal and modified.

model E_2 and simultaneously increasing Young's modules of the front half to $E_1 = 2E_0 - E_2$, where E_0 is the original Young's module. In this way we kept the fin-bending frequency at its original value.

Figure 8 shows the flutter velocity of the clamped fin, at $DC = 0$, vs the ratio E_2/E_0. It can be observed that reducing the rear chordwise stiffness increases the flutter velocity, as expected. Figure 9 shows the flutter velocity as a function of the lifting force generated by the fin for the original model ($E_2/E_0 = 1.0$) and for the modified one, where $E_2/E_0 = 0.1$. A significant increase of the flutter velocity is achieved (up to 10%) without degrading missile maneuverability.

Full Missile Model

Because the fins are typically very light compared with the entire missile, a separate analysis of the clamped fin is usually sufficient for fin flutter investigation. The entire missile model of Fig. 1b was used in this work to analyze missile response to control commands and to investigate the effect of the pneumatic system frequency f_p, typically in the range of 15–40 Hz, on the dynamic response and stability. The nominal pneumatic frequency is $f_p = 25$ Hz. The flutter velocity of the movable fin with $DC = 50\%$ is about 1400 m/s. A typical stable time response of the fin-root angle to pneumatic step command is shown in Fig. 10. The response exhibits three types of oscillations. The larger are short-period oscillations

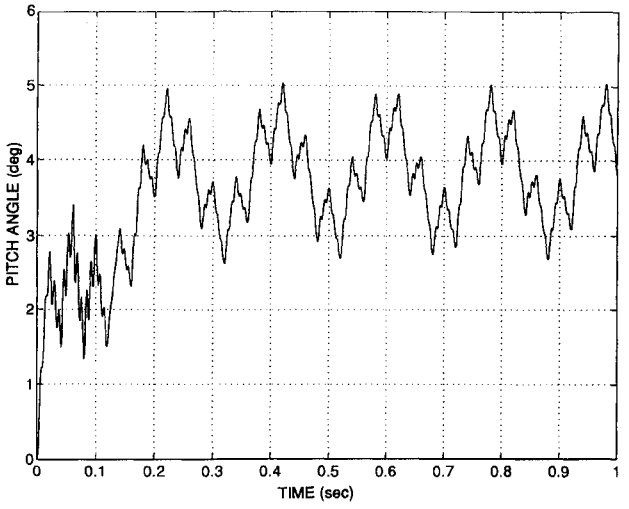

Fig. 10 Fin angle response to step command in full-missile case at U = 1300 m/s with f_p = 25 Hz.

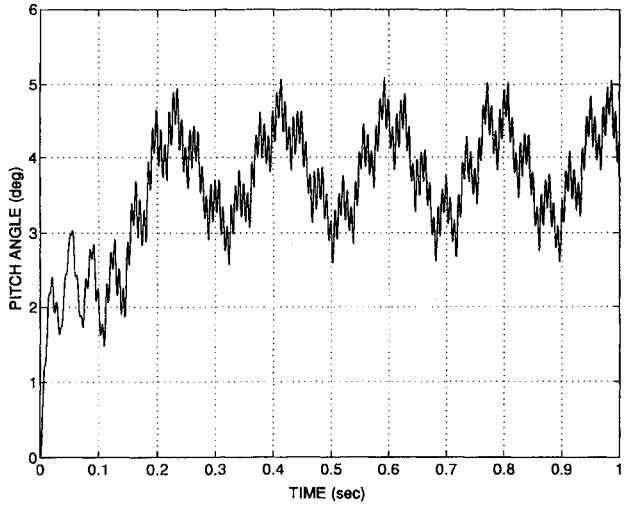

Fig. 11 Fin angle response to step command in full-missile case at U = 1300 m/s with f_p = 28 Hz.

of about 4.5 Hz with very small damping. On top of these, we see the 25 Hz pneumatic oscillations, with noise of about 200 Hz, which is related to the fin-pitch frequency. As in the case of fin flutter, the low-frequency short-period response is also affected by the hinge moment through changes in the static aeroelastic effects on the aerodynamic stability coefficients.

Figure 11 shows the same response as in Fig. 10, but with pneumatic frequency of 28 Hz, which is identical to the first bending frequency of the missile body. The match between the bending and pneumatic frequencies causes a slight increase in the amplitude of the pneumatic oscillations. A larger increase is observed in the 200 Hz fin-pitch oscillations. This increase appears at all velocities larger than about 1000 m/s (not shown). It is a result of the nonlinear interaction between the pneumatic dynamics and the missile bending dynamics, which is not shown in linearized analyses. This interaction also reduced the flutter velocity by about 2.5%.

Conclusions

Time-domain state–space equations of motion for the simulation of dynamic aeroelastic response of missiles with nonlinear pneumatic control systems were developed. Time-marching solutions at various velocities and actuator commands were required to analyze the system stability. It was shown that the fin flutter velocity is strongly dependent on the pneumatic cylinder pressure which controls the missile maneuvers. The fundamental flutter mechanism involves the fin pitch mode, whose low frequency increases with the cylinder pressure and with the flow dynamic pressure and the first fin bending mode. The pneumatic oscillations do not allow easy computation of modal damping values from the time response. Nevertheless, the flutter boundaries can be indicated by the appearance of beating oscillations. An equivalent spring, based on a typical nonlinear time response, can replace the pneumatic system in linear frequency-domain flutter analysis for better understanding the flutter mechanism and for efficient establishment of keep-out zones. However, a conservative approach should be taken because the linearized analysis can be significantly inaccurate. The friction between the O-ring of the piston and the cylinder has a positive influence on the dynamic stability of the fin, but the increased flutter velocity was, in our case, more sensitive to the maneuver command. The full-missile example showed that closeness between the pneumatic frequency and the first natural frequency of the missile body can cause high-frequency structural oscillations, but there was a negligible effect on the flutter velocity. It was demonstrated that fin flutter velocity can be increased significantly by introducing chordwise flexibility in the rear part of the fin.

References

[1]Greif, H. D., "Describing Function Method of Servomechanism Analysis Applied to Most Commonly Encountered Nonlinearities," *AIEE Transactions*, Pt. 2, No. 8, 1953, pp. 243–248.

[2]Laurenson, R. M., and Trn, R. M., "Flutter Analysis of Missile Control Surfaces Containing Structural Nonlinearities," *AIAA Journal*, Vol. 18, No. 10, 1980, pp. 1245–1251.

[3]Lee, C. L., "An Iterative Procedure for Nonlinear Flutter Analysis," *AIAA Journal*, Vol. 24, No. 5, 1985, pp. 833–840.

[4]Girard, D. D., "Nonlinear Flutter Analysis of a Missile Fin/Actuator," IEEE Paper TP4 4:00, April 1986.

[5]Andersen, B. W., *The Analysis and Design of Pneumatic Systems*, Robert Krieg, New York, 1976, Chap. 2.

[6]Bisplinghoff, R. L., Ashley, H., and Halfman, R. L., *Aeroelasticity*, Addison–Wesley, Reading, MA, 1955, Chap. 10.

[7]Rodden, W. P., and Johnson, E. H., "MSC/NASTRAN Aeroelastic Analysis User's Guide," MacNeal Shwendler Corp., Los Angeles, CA, 1994.

[8]Tiffany, H., and Adams, W. M., Jr., "Nonlinear Programming Extensions to Rational Function Approximation Methods for Unsteady Aerodynamic Forces," NASA TP 2776, July 1988.

[9]Karpel, M., "Time-Domain Aeroservoelastic Modeling Using Weighted Unsteady Aerodynamic forces," *Journal of Guidance, Control, and Dynamics*, Vol. 13, No. 1, 1990, pp. 30–37.

[10]Karpel, M., and Wieseman, C. D., "Modal Coordinates for Aeroelastic Analysis with Large Local Structural Variations," *Journal of Aircraft*, Vol. 31, No. 2, 1994, pp. 396–403.

[11]Karpel, M., and Wieseman, C. D., "Time Simulation of Flutter with Large Stiffness Changes," *Journal of Aircraft*, Vol. 31, No. 2, 1994, pp. 404–410.

[12]Dillenius, M. F. E., Canning, T. N., Lesieutre, T. O., and McIntosh, S. C., "Aeroelastic Tailoring Procedure to Optimize Missile Fin Center of Pressure Location," AIAA Paper 92-0080, Jan. 1992.